



Research paper

A metabolomics approach to reveal the mechanism of developmental toxicity in zebrafish embryos exposed to 6-propyl-2-thiouracil

Pia Wilhelmi^{a,b,*}, Varun Giri^{a,**}, Franziska Maria Zickgraf^{a,***}, Volker Haake^c, Stefan Henkes^c, Peter Driemert^c, Paul Michaelis^d, Wibke Busch^d, Stefan Scholz^d, Burkhard Flick^{a,1}, Marta Barenys^{b,e}, Barbara Birk^a, Hennicke Kamp^c, Robert Landsiedel^{a,f}, Dorothee Funk-Weyer^a

^a BASF SE, Experimental Toxicology and Ecology, 67056, Ludwigshafen am Rhein, Germany

^b University of Barcelona, Research Group in Toxicology-GRET, 08028, Barcelona, Spain

^c BASF Metabolome Solutions, 10589, Berlin, Germany

^d Helmholtz Centre for Environmental Research-UFZ, Department of Bioanalytical Ecotoxicology, 04318, Leipzig, Germany

^e German Centre for the Protection of Laboratory Animals (Bf3R), German Federal Institute for Risk Assessment (BfR), 10589, Berlin, Germany

^f Free University of Berlin, Institute of Pharmacy, Pharmacology and Toxicology, 14195, Berlin, Germany



ARTICLE INFO

Keywords:

Developmental toxicity
Metabolomics
Zebrafish embryo
Thyroid disruption

ABSTRACT

A crucial component of a substance registration and regulation is the evaluation of human prenatal developmental toxicity. Current toxicological tests are based on mammalian models, but these are costly, time consuming and may pose ethical concerns. The zebrafish embryo has evolved as a promising alternative model to study developmental toxicity. However, the implementation of the zebrafish embryotoxicity test is challenged by lacking information on the relevance of observed morphological alterations in fish for human developmental toxicity. Elucidating the mechanism of toxicity could help to overcome this limitation. Through LC-MS/MS and GC-MS metabolomics, we investigated whether changes to the endogenous metabolites can indicate pathways associated with developmental toxicity. To this aim, zebrafish embryos were exposed to different concentrations of 6-propyl-2-thiouracil (PTU), a compound known to induce developmental toxicity. The reproducibility and the concentration-dependence of the metabolome response and its association with morphological alterations were studied. Major morphological findings were reduced eye size, and other craniofacial anomalies; major metabolic changes included increased tyrosine, pipercolic acid and lysophosphatidylcholine levels, decreased methionine levels, and disturbance of the 'Phenylalanine, tyrosine and tryptophan biosynthesis' pathway. This pathway, and the changes in tyrosine and pipercolic acid levels could be linked to the mode of action of PTU, i.e., inhibition of thyroid peroxidase (TPO). The other findings suggested neurodevelopmental impairments. This proof-of-concept study demonstrated that metabolite changes in zebrafish embryos are robust and provide mechanistic information associated with the mode of action of PTU.

1. Introduction

The approval of new substances is subject to strict regulations. In Europe, for instance, this is included in legislative frameworks such as REACH [1] and EudraLex [2]. Based on the foreseen use and/or the production quantities, these regulations require standard information on

toxicological hazards. These data are mostly generated by animal testing. At least since the thalidomide tragedy in the 1960s it is widely known that chemicals can cross the placental barrier and irreversibly harm the developing organism [3]. Therefore, testing for developmental toxicity is an integral part of the regulatory risk assessment. Recent regulations recommend testing in two mammalian species, rats and rabbits [4,5], to provide information on developmental toxicity.

* Corresponding author.

** Corresponding author.

*** Corresponding author.

E-mail addresses: pia-rosa-maria.wilhelmi@basf.com (P. Wilhelmi), varun.giri@basf.com (V. Giri), franziska-maria.zickgraf@basf.com (F.M. Zickgraf).

¹ Present address: NUVISAN ICB GmbH, Toxicology, 13353 Berlin, Germany.

Abbreviations	
AOP	adverse outcome pathway
c	concentration
CRYM	μ -crystallin
EC	effective concentration
FC	fold change
FDR	false discovery rate
FET	zebrafish embryo acute toxicity test
GC	gas chromatography
GC-MS	gas chromatography-mass spectrometry
HILIC	hydrophilic interaction liquid chromatography
hpf	hours post fertilization
KEGG ID	Kyoto Encyclopedia of Genes and Genomes identifier
LC _x	x % lethal concentration
LC	liquid chromatography
LC _{in}	liquid chromatography lipid negative ionization mode
LC _{ip}	liquid chromatography lipid positive ionization mode
LC-MS/MS	liquid chromatography-tandem mass spectrometry
LC _{p_n}	liquid chromatography polar negative ionization mode
LC _{p_p}	liquid chromatography polar positive ionization mode
LPC	lysophosphatidylcholine
LPE	lysophosphatidylethanolamine
Mfsd2a	major facilitator superfamily domain-containing protein 2A
PC	phosphatidylcholine
PCA	principal component analysis
PCx	principal component x
PE	phosphatidylethanolamine
PoD	point of departure
PPAR γ	peroxisome proliferator-activated receptor gamma
PTU	6-propyl-2-thiouracil
SD	standard deviation
T3	triiodothyronine
T4	thyroxine
TAG	triacylglycerol
TG	test guideline
TPO	thyroid peroxidase

Ethical and economic considerations, as well as the need for a better understanding of toxicity mechanisms represent major drivers to move away from mammalian testing and develop alternative methods [6–8]. The throughput of current mammalian-based testing is insufficient to obtain information on all chemicals in commerce and to match the pace of development of new compounds [9]. In addition, a major limitation of the regulatory accepted developmental toxicity tests is that they only provide information about the apical outcome, but not about the molecular and cellular changes that precede this outcome. Alternative methods could fill these information gaps and shed light on the toxicity mechanisms, thereby paving the way from an apical to a more mechanistic assessment [10].

The zebrafish embryo has emerged as a promising alternative model to study various aspects of developmental toxicity [11–13] given that it represents a complex vertebrate model. Several animal welfare regulations consider the use of embryonic life stages as unprotected non-sentient stages. Therefore, European regulations allow the use of zebrafish embryos up to 5 days post fertilization, when independent feeding starts, as an alternative to animal testing [14,15]. Their rapid embryonic development and small size make them an attractive medium-to high-throughput screening system. Based primarily on a morphological evaluation, the zebrafish has already shown a good concordance with mammalian data regarding the classification of substances as developmentally toxic [16–18].

With the assessment of morphology alone, however, it is difficult to extract mechanistic information. By applying targeted mass spectrometry-based techniques, the metabolome and thus the physiological or pathological state of an organism can be captured [19]. Since metabolites play important roles in all molecular processes, e.g., as signal transducers, building blocks or fuel, an altered metabolome can indicate impaired pathways, associated with diverse toxicological endpoints. Based on this, metabolic effect patterns have already been described for various endpoints such as maternal or liver toxicity in rat plasma and in *in vitro* systems [20–24]. It has further been demonstrated in zebrafish that altered endogenous metabolite levels can be indicative of developmental toxicity [25].

Using a combination of automated phenotype analysis and targeted mass spectrometry-based metabolomics, the morphological and mechanistic effects of exposure to 6-propyl-2-thiouracil (PTU), a model compound of developmental toxicity, were investigated in zebrafish. PTU is a pharmaceutical, which is prescribed to treat hyperthyroidism [26]. It inhibits thyroid peroxidases (TPO) [27] and deiodinases [28, 29], which results in a reduced availability of the thyroid hormones

triiodothyronine (T3) and thyroxine (T4). The teratogenic potential of PTU has been demonstrated by Benavides et al. [30], who reported delayed neural tube closure and cardiac abnormalities in mice. In addition, PTU-induced developmental neurotoxicity was reported in rats [31], though, they were not accompanied with adverse structural changes. Zebrafish, on the other hand, exhibited structural changes after treatment with PTU in previous studies [32,33].

The aim of the present study was to investigate if the metabolic response of PTU-treated zebrafish embryos can be correlated with developmental toxicity. For this purpose, the suitability of the zebrafish matrix for metabolomics was tested in terms of obtaining reproducible results, and the morphological and metabolic changes were examined as indicators of developmental toxicity. The results provided crucial evidence for the link between PTU-related effects, thyroid hormone disruption and neurodevelopment, meanwhile demonstrating the applicability of the concept to identify developmental toxicity.

2. Material and methods

2.1. Material

All reagents were purchased from Merck unless otherwise stated. The test chemical 6-propyl-2-thiouracil (PTU; CAS no. 51-52-5) had a minimum purity of 99%.

2.2. Test system

Embryos from an in-house wild-type zebrafish (*Danio rerio*) strain Obi/Wik produced at the Helmholtz Centre for Environmental Research-UFZ (Leipzig, Germany) were used for morphology and metabolome analysis. The adult fish were cultured at 26 °C in tanks with recirculating water and maintained on a day/night cycle of 14/10 h. For egg production, trays with artificial plants were placed overnight in the tanks. After spawning, eggs were manually selected under the microscope. Only intact fertilized eggs in approximately 8-cell stage were used for subsequent exposure. Fish were cultured according to German and European animal protection standards approved by the government of Saxony (Landesdirektion Leipzig, Germany, Aktenzeichen 75–9185.64).

2.3. Exposure conditions

Stock solutions of PTU were prepared in DMSO. Stocks were further diluted in exposure medium (2 mM CaCl₂, 0.5 mM MgSO₄, 0.75 mM

NaHCO₃ and 0.07 mM KCl, pH 7.4-7.5) according to the OECD test guideline (TG) 236 [34]. The final DMSO concentration in the test medium was 0.01%. Zebrafish were exposed from 8-cell stage until 96 h post fertilization (hpf) at 28 ± 1 °C. For concentration range-finding and morphology analysis, one embryo per well was seeded in 400 µL of the test medium on a 96-square well plate with 16 embryos per concentration. For metabolome samples, embryos were exposed in glass vials, each containing 50 embryos in 50 mL test medium.

2.4. Concentration-range finding

Fifteen concentrations between 325 and 3980 µM were tested in three independent replicates. The concentrations were selected based on available information for a 48-120 hpf exposure window [35] and by applying a geometric scale with factors of 2.3 and 1.5 in subsequent replicates to obtain data points in the range of effect concentrations. Using a dissection microscope, mortality levels were determined as described in the OECD TG 236 [34]. Gross morphological changes were assessed by microscopical observations and scoring (presence or absence of phenotype). To model the concentration-dependency of lethal or sublethal endpoints, a curve was fit with non-linear regression and a confidence level of 95% using GraphPad Prism 8.0.2.

2.5. Morphology analysis

A total of ten concentrations of PTU ranging from 16.5 to 2309 µM and one solvent control (0.01% DMSO) were tested in two independent replicates. The concentrations were selected based on the results of the range finding by applying a geometric scale with a factor of 1.7 and including low concentrations to identify potential subtle morphological effects. 24 embryos were exposed per condition but due to loss of specimen during the automated imaging, the number of fish subjected to quantitative imaging ranged between 16 and 20. At 96 hpf, prior to the assessment of morphology, larvae were anaesthetized by adding 20 µL of a tricaine solution (600 mg/L MS-222 in 0.01 M TRIS, pH 7) to each well. Using a VAST bioimager (Union Biometrica, Aalst, Belgium) each fish was automatically positioned in a glass capillary and images were obtained of lateral and dorsoventral views with a digital camera of 10 µm resolution.

The images were annotated, and features were quantified using the FishInspector software [36,37]. The used version (1.7) represents a modification of the published open-source version [36] using feature annotations based on deep-learning models (details on the modified software will be published elsewhere, a free license is available on request). Relevant morphological changes were identified by comparing feature metrics between PTU exposed fish and controls. A change was considered relevant when it was outside the threshold of 1.5 fold of the standard deviation (SD) of the corresponding control feature. The percentage of embryos deviating from controls was used to determine the EC₅₀ (50% effective concentration) for each feature. The EC₅₀ was only calculated for features that exhibited a concentration-response relationship (indicated by comparison of the Akaike information criterion to a linear model with slope 0, by application of the Tukey trend test, and by a minimum of 25% embryos showing the effect).

Subsequently, features were translated into corresponding ontologies using ONTOBEE [38]. Whenever possible, existing ontologies were used. In some cases, new ontology terms were developed based on existing anatomical terms and qualifiers (subject to submission to ONTOBEE). If several features were relating to the same ontology term, the most sensitive term was used for the EC₅₀ calculation. A list of feature metrics and translations to zebrafish ontology terms can be found in the supplementary (Table S1).

2.6. Sample generation for metabolomics

Exposure concentrations of 325, 487, 731, 1640, and 3700 µM were

used for metabolome analysis. These concentrations were selected based on lethality concentrations (LC_x) from the range-finding tests: The highest test concentration (c5) was based on the LC₂₅ (lethal concentration 25%), the second highest (c4) oriented on the LC₁₀, further concentrations were selected representing a dilution factor of 1.5 and considering morphological effects. A solvent control containing 0.01% DMSO was included. Each exposure was performed in four parallel technical replicates with 50 pooled embryos. Embryos were visually checked daily, and dead embryos were removed and replaced with embryos from an additional technical replicate prepared as backup to ensure the same number of embryos per replicate. The exposure was terminated at 96 hpf by washing with isotonic saline. Afterwards, samples were freeze-dried and stored at -80 °C. The whole experiment was repeated on a different day to test for reproducibility.

2.7. Targeted mass-spectrometry based metabolomics

GC-MS (gas chromatography-mass spectrometry) and LC-MS/MS (liquid chromatography-tandem mass spectrometry) with targeted multiple reaction monitoring were applied for a semi-quantitative targeted metabolite profiling.

Samples were extracted each with 1500 µL of extraction buffer (methanol, dichloromethane, water, and toluene (93:47:16.5:1, v/v) buffered with ammonium acetate and including internal standards) and homogenized using a ball mill (Bead Ruptor, Biolab). Homogenates were centrifuged (15294xg, 10 min, 12 °C) to precipitate proteins and debris. A 100 µL aliquot of the supernatant extract was subjected to LC-MS/MS. Each 2.5 µL of extract were injected for reversed-phase and hydrophilic interaction liquid chromatography (ZIC - HILIC, 2.1 × 10 mm, 3.5 µm, Supelco) followed by MS/MS detection (AB Sciex QTrap 6500+) using the positive and negative ionization mode. For reversed-phase high performance liquid chromatography (RP-HPLC, Ascentis Express C18, 5 cm × 2.1 mm, 2.7 µm Supelco), gradient elution (0 min-100% A; 0.5 min-75% A, 25% B; 5.9 min-10% A, 90% B; 600 µL/min) was applied using (A) water/methanol/0.1 M ammonium formate (1:1:0.02 w/w) and (B) methyl-tert-butylether/2-propanol/methanol/0.1 M ammonium formate (2:1:0.5:0.035 w/w) with 0.5% (w %) formic acid. HILIC gradient elution (0 min-100% C; 5 min-10% C, 90% D; 600 µL/min) was applied using (C) acetonitrile/water (99:1, v/v) and 0.2 (v %) acetic acid and (D) 0.007 M ammonium acetate with 0.2 (v %) acetic acid.

For GC analysis, water was added (3.75:1, v/v) to another aliquot of the extract, which resulted in a separation of the polar (upper phase, 400 µL) and lipid (lower phase, 90 µL) phases. Using GC-MS (GC7890-5975 MSD, Agilent Technologies), both phases were analyzed after derivatization as described in Ref. [39]. In summary, the lipid fraction was initially supplemented with methanol under acidic conditions to produce fatty acid methyl esters, derived from free fatty acids and hydrolyzed complex lipids.

The polar and lipid fractions were both further derivatized with *O*-methyl-hydroxylamine hydrochloride and with a silylating agent (*N*-methyl-*N*-(trimethylsilyl) trifluoroacetamide). Finally, 0.5 µL of each derivatized extract were used for analysis. Samples were measured in a randomized sequence design to prevent artificial results in terms of analytical shifts.

2.8. Metabolomics data processing

For GC-MS and LC-MS/MS profiling, data were normalized to the median of reference samples (so called pools) to account for inter- and intra-instrumental variation. The pools were generated from a large independent collection of untreated zebrafish embryos, processed and measured in parallel with the study samples. Quality of data was checked at two levels: insufficient quality resulted in exclusion of analytes and/or samples. To overcome any systematic batch effects, the metabolite measurements for each experiment were normalized to the median of the respective controls.

In total, 264 metabolites were measured from which 249 were annotated. As some metabolites were detected with different analytical methods (GC-MS and LC-MS/MS lipid/polar positive/negative mode), the total number of annotated metabolites without duplicates was 230. Duplicates were not excluded to validate reproducibility and to ensure better comparability with other datasets. The measured metabolites covered a wide range of biochemical classes including acylglycerols, amino acids, carbohydrates, glycerophospholipids, energy metabolism related, miscellaneous, nucleobases, fatty acids, lysoglycerophospholipids, signal substances, sphingolipids, and vitamins. For some analytes, listed as 'unknown', no clear identification was possible. These were still included in the analysis because analytical information is growing, which may allow an identification at a later date.

2.9. Multi- and univariate analysis of metabolomics data

Multi- and univariate statistical analyses were conducted to reveal metabolic effect patterns of PTU exposure. An unsupervised principal component analysis (PCA) was performed in R Statistical Software [40]. The data for each metabolite were log-transformed, then scaled by subtracting the mean value of the metabolite, and divided by the SD. Metabolites detected in less than 20% of all samples were excluded. The remaining missing values were imputed by a k-nearest-neighbors (knn) algorithm using `impute.knn` function from the R-package `impute` [41]. The function `prcomp` was used for computing the PCA and the package `ggplot2` [42] was used for visualization.

A concentration-dependent response was modeled based on PC1 values obtained from the PCAs computed independently for each experimental run. PC1 values for each sample were plotted against the test concentration and a three-parameter log-logistic model was fitted through the data, using `drc` package [43]. A confidence interval of 95% was used for the curve and the control variability was defined by the 2.5% and 97.5% quantiles, which corresponded to 95% spread in the control samples. The point of departure (PoD) marks the concentration at which the confidence interval of the curve and the corresponding quantile of the controls separate, i.e., the curve with its 95% confidence has crossed the 95% spread of the controls.

For identification of potentially discriminating metabolites, a univariate analysis was performed by combining fold change variations with statistical significance using Wilcoxon signed-rank test. Fold changes were calculated relative to the respective control and based on the median of replicates in each experiment. A significance threshold of $p \leq 0.1$ was used as this has been shown to be useful for the detection of changes in metabolite patterns [44].

2.10. Concentration-response modelling of individual metabolites

To compare the sensitivity of individual metabolite responses with respect to PTU exposure, concentration-response curves were modeled for each metabolite based on a maximum likelihood approach implemented in the R [40] package `drc` version 3.0.1 [43]. All replicates from both experiments were combined to provide a robust curve fit. The data was normalized to the mean of the controls and subsequently log2 transformed. Three models, namely generalized log-logistic, Weibull I, and Cedergreen-Ritz-Streibig were applied [43]. The best fitting model was determined via Akaike information criterion (AIC). A confidence interval of 95% was used for the curve and the control variability was described by the 2.5% and 97.5% quantiles. The PoD marks the concentration at which the confidence interval of the curve and the corresponding quantile of the controls separate for the first time.

2.11. Metabolic pathway analysis

Metabolite changes were also considered in a broader context by connecting them to metabolic pathways. For pathway analysis, a web-based tool, which is incorporated into MetaboAnalyst 5.0 platform

was used [45,46]. First, the metabolites were translated to KEGG IDs (Table S3). When several metabolites were assigned to the same ID, the metabolite that showed the highest significance of change across all concentrations was selected for pathway analysis. Consequently, the total number of metabolites assigned to a unique KEGG ID was 109. Second, metabolite intensities for all conducted replicates were uploaded as a concentration table. Metabolites with greater than 20% of missing values were removed and remaining missing values were estimated using a knn algorithm. The enrichment method selected was global test, the topology analysis selected was relative-betweenness centrality, and for pathway library *Danio rerio* was chosen. The reference metabolome, containing all measured metabolites was uploaded. Third, a false discovery rate (FDR) threshold of <0.25 was applied to filter out the significantly affected pathways.

In addition to the intensity of changes in the measured metabolites, their relative position in the pathway was considered and translated into an impact value. The impact is a measure for the importance of the measured metabolites with respect to all metabolites in the respective pathway and is calculated based on relative-betweenness centrality [47]. The impact of a pathway results from summing the relative-betweenness centrality values of all measured metabolites and normalizing it to that of all metabolites. An impact closer to 1 indicates that a large fraction of the metabolites in the pathway were measured or that the set of measured metabolites are more central and a change to them may have strong influence on the entire pathway. Whereas a low impact value indicates a few measured metabolites and/or that they are rather peripheral in the pathway.

3. Results

3.1. PTU induces morphological effects in the absence of lethality

To determine the concentrations for the subsequent automated phenotype analysis and metabolomics, initial concentration range-finding tests were performed. In total, 15 concentrations were screened to enable a robust curve fitting. A clear separation was observed between cumulative sublethal effects, such as edema or low pigmentation (based on scoring from microscopical observations), and lethal effects (Fig. 1). While sublethal effects occurred from 1100 μM , lethality was observed only from 3300 μM . For metabolome analysis, concentrations were selected aiming for low general toxicity. The

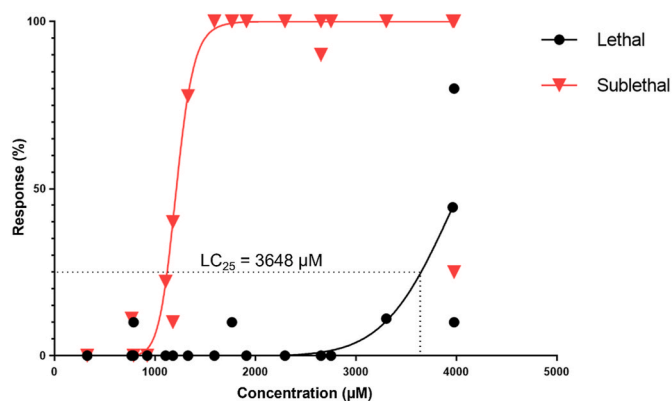


Fig. 1. Concentration-response relationship based on lethal and sublethal effects for PTU exposed zebrafish embryos at 96 h post fertilization.

The percentage of dead fish, lethal effects, depicted as circles, and the percentage of surviving fish with one or more gross morphological changes, sublethal effects, depicted as triangles, were recorded and a curve was fitted. The figure shows that the sublethal maximum effect was reached at about 1600 μM , at which no lethality was observed. Based on these results, the concentration range for metabolomics was determined, using LC_{25} (lethal concentration 25%) as the highest test concentration.

highest concentration was set to correspond to the LC₂₅ level in the range-finding test.

3.2. The swim bladder and eyes are the organs most sensitive to PTU exposure

An image-based quantitative assessment of phenotypes was applied to describe morphological alterations associated with PTU exposure. Using annotated features, EC₅₀-values for morphological endpoints were determined. At concentrations below 1000 µM, the endpoints ‘eye decreased area’ (EC₅₀ = 818 µM) and ‘swim bladder absent’ (EC₅₀ = 124 µM) were noted to be affected in 50% of the treated zebrafish embryos (Fig. 2). At higher concentrations, the whole organism length decreased (EC₅₀ = 1049 µM) and further features such as the yolk, craniofacial structures (e.g., eye decreased distance posterior otolith, eye decreased distance eye, mouth increased angle to posterior otolith), and the pectoral fins were affected. The EC₅₀ for pigmentation, notochord curvature and pericardium size were not reached within the concentration range tested. However, a concentration-dependent response was recognized. Thus, the most sensitive structures of zebrafish embryos exposed for 96 h to PTU were the swim bladder and the eyes.

3.3. The metabolome reveals concentration-dependent and reproducible effects

For a global evaluation of the concentration-dependent effects of the zebrafish metabolome and its reproducibility, a principal component analysis (PCA) was performed. In the PCA, the replicates of the two independent experiments clustered together at their respective concentrations (Fig. 3A), showing a reproducibility of effects. The data preprocessing was designed to remove systematic batch effects. Absence of strong differences between the experimental runs in the PCA, indicate the absence of specific batch effects. 48% of the variability was explained by the first two PCs, 34% by PC1 and 14% by PC2. Test concentration c5 was the strongest contributor to the separation in PC1. The loadings plot (Fig. 3B) revealed the metabolites that made the greatest impact on the separation of the samples in the PCA. It identified metabolites from the class of amino acids and related, and lysoglycerophospholipids as the main discriminating factors in PC1.

The greatest variation in the metabolome data was covered in PC1, which separated the concentration groups. To capture this concentration-response relationship, PC1 values for each replicate were plotted against the concentrations tested and the PoD was determined (Fig. 4), representing the onset of a global change in the metabolome. In

both experiments, c3 represented the test concentration closest to the PoD. Since the onset of a change in the whole metabolome was anticipated to be associated with specific effects, the test concentration c3 was used as reference for some of the analyses of individual metabolite alterations.

3.4. Amino acid- and lysoglycerophospholipid-related changes shape the metabolic effect pattern

When individual metabolite alterations were examined, metabolites significantly changed in c3 (Table 1) represented the onset of a global metabolome change based on the PCA-derived PoDs. The fold change (FC) table illustrates the direction and intensity of the metabolite changes compared to the controls and shows how this effect continues at further test concentrations. Predominantly amino acids and related were found among the most altered metabolites in c3. Highly elevated levels of pipercolic acid were measured in both experiments (FC of 2.06 and 1.91), and of tyrosine in experiment 1 (FC of 1.87 and 1.79). Strongly reduced levels were noticed for fructose-6-phosphate in experiment 1 (FC of 0.29). In addition, methionine was decreased by about one-third in experiment 2 (FC of 0.65).

A consistent trend in concentration dependency in the direction of most metabolite changes was observed, though not always statistically significant in both experiments at one concentration. For example, a discernible trend towards an increase in lysoglycerophospholipids was observed in both experiments at c3. Tyrosine demonstrates a distinct concentration-response relationship with continuously increasing FCs up to c4 and decreasing at c5 in both experiments and for both analytes. Furthermore, a switch in the direction of change between c4 and c5 was noticed for some metabolites, such as LPC (C20:5, C20:4, C18:2), LPE (C22:6), histidine, 2'-deoxycytidine, and phenylalanine. The consistency of these changes between experiments adds evidence to the reproducibility of the data.

To ascertain quantitatively the reproducibility, the correlation of FCs between the two experimental runs was computed. The pairwise Pearson correlations (r) between respective concentrations (c1 to c5) from the two experiments were found to be 0.52 (p < 0.01), 0.22 (p = 0.14), 0.65 (p < 0.01), 0.99 (p < 0.01), and 1.0 (p < 0.01) calculated for the selection of metabolites reported in Table 1 (for correlation based on all metabolites see Fig. S2). The weaker correlation at the low concentrations is due to relatively few changes in the metabolome.

In addition to considering the significantly altered metabolites at c3, which represent a general deviation of the metabolome from controls, we took a second approach aiming to extract the metabolites with mechanistic information. This approach determined the concentration

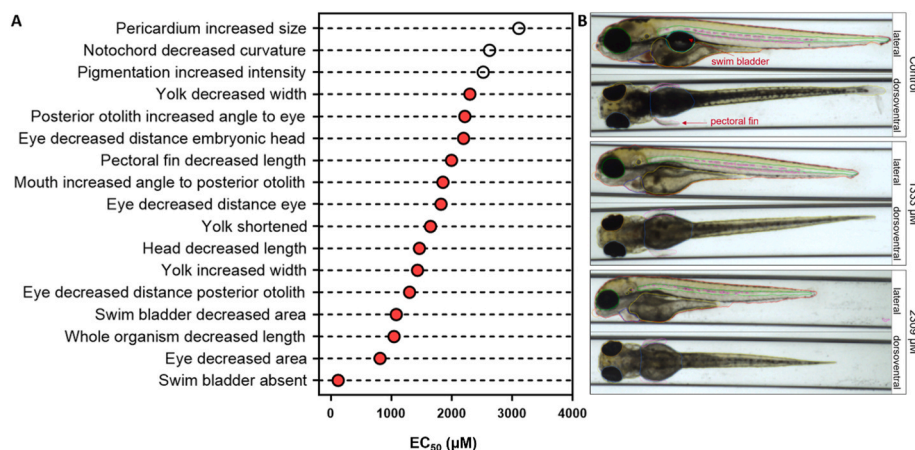


Fig. 2. 50% effective concentration (EC₅₀) of morphological alterations in zebrafish embryos after PTU exposure for 96 h.

Automated imaging and feature annotation was used to identify morphological alterations for each embryo at the end of the experiment. For each morphological alteration, the concentration at which the 50% effect level would be reached was calculated. A) EC₅₀-values were derived for all endpoints exhibiting a concentration-response relationship. For some endpoints (unfilled circles) the EC₅₀ values represent an extrapolation since the maximum observed effects were below 50%. Values can be found in supplementary (Table S2). B) Representative images of phenotypes from the two highest concentrations tested and a solvent control are shown in lateral and dorsoventral positions. Colored lines indicate Fish-Inspector feature metrics. The most sensitive endpoint was the absence of the swim bladder. Swim bladder and pectoral fin are indicated by an arrow in the control.

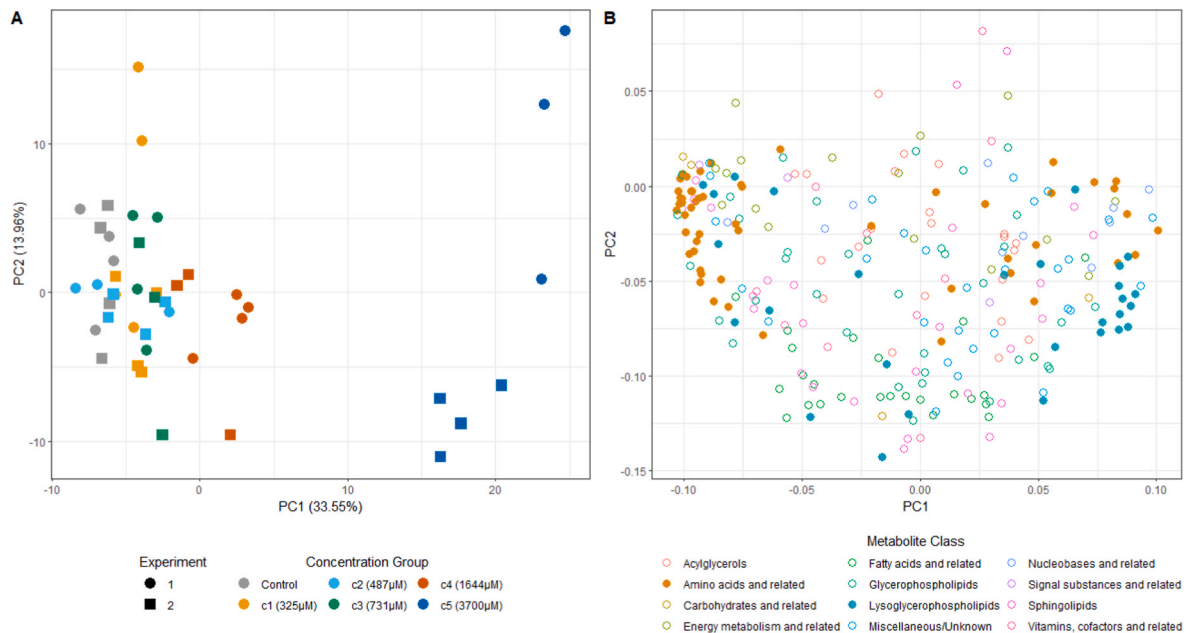


Fig. 3. Principal component analysis (PCA) of the metabolome response of PTU-exposed zebrafish embryos in two independent experiments. We used PCA to assess the global metabolome response. The first two dimensions are shown, representing about 48% of the response. A) PCA plot of metabolome data from the two experiments. Colors depict exposure concentrations and symbols depict experimental runs. A concentration-dependent response along PC1 (explaining 34% variability) was observed. Only for the highest test concentration (c5) a separation between the two experiments was noticed along PC2 (explaining 14% variability). Though for test concentrations c1-c4 no clear separation between experiments was perceived. B) PCA loadings plot showing the strongest drivers for the separation in PC1. Among them were many decreased amino acids and increased lysoglycerophospholipids (filled circles).

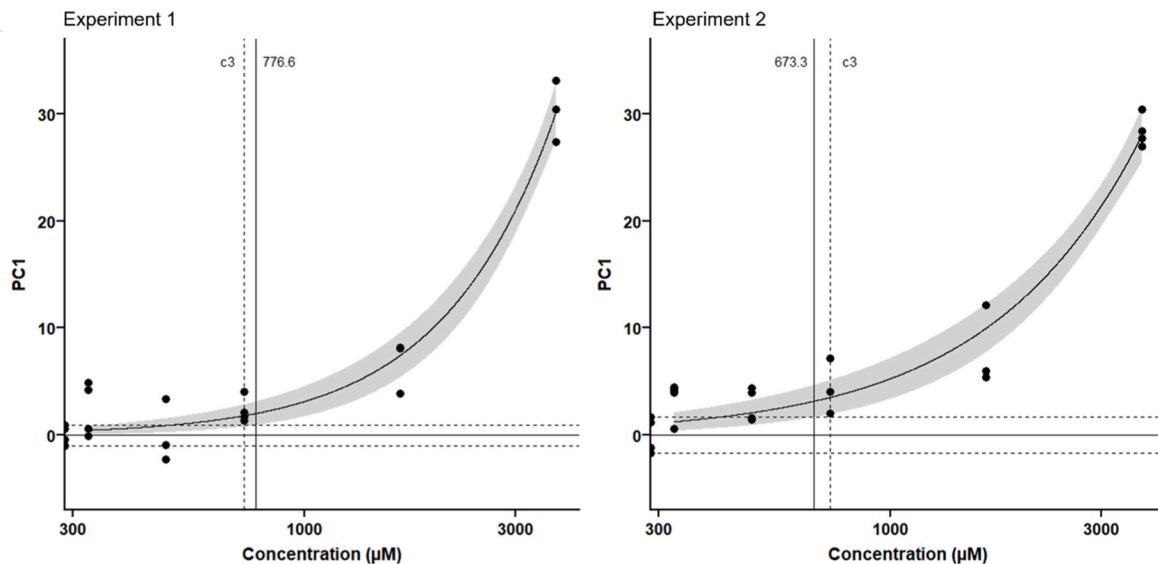


Fig. 4. Determination of the point of departure (PoD) to identify the onset of an overall change in the metabolome. Global metabolite changes as estimated by principal component analysis (PCA) exhibit exposure concentration dependency. To model the concentration response, PC1 values were computed independently for each of the two metabolomics experiments (see Fig. S1 for corresponding PCA plots). PC1 values of each replicate were plotted against the respective test concentration and a curve was fitted. The spread of controls is marked by the horizontal dashed lines, which represent the 2.5% and 97.5% quantiles; the mean is represented as horizontal solid line. The grey shaded area indicates the 95% confidence interval (CI) of the curve. The PoD marks the concentration at which the curve deviates with high confidence from control variability (marked by a vertical solid line). The dashed vertical line marks the test concentration c3, which is closest to the PoD and was therefore regarded as the onset of a global change in the metabolome.

at which each individual metabolite first exceeded control variability (Fig. 5A). The most sensitive metabolites representing a PoD below test concentration c2 (487 µM) were LPC (C18:2) (LC_{ln}), pipercolic acid, isoleucine, TAG (C32:1, C16:1), and asparagine. An advantage of this approach is that it also reveals metabolites which were not significantly changed at c3 but still exhibit a concentration-dependent response. This

was the case with e.g., TAG (C32:1,C16:1), LPC (C14:0), LPC (C20:2), *trans*-4-hydroxyproline, PE (C34:0), and uric acid.

Although the statistical method was different, a large overlap was seen between the metabolites detected in the first (Table 1) and second approaches (Fig. 5). When comparing the top 25 metabolites with the lowest PoD, 19 of them were also found in the first approach.

Table 1

Fold changes of metabolites at test concentrations c1-c5 based on the selection of significantly altered metabolites in c3. Zebrafish embryos were exposed to five concentrations (c1-c5) of PTU in two independent experiments. A total of 264 metabolites were measured. Only metabolites significantly ($p \leq 0.1$) changed at c3 in at least one experiment are presented here (full list can be found in Table S3). Fold changes were computed relative to the respective control, with the color code indicating the direction and intensity of change (blue - decrease; red - increase) and font style indicating the significance level (see legend below). The table is sorted in descending order by the significant fold changes in c3.

GC - gas chromatography; LC - liquid chromatography; LPC - lysophosphatidylcholine; LPE - lysophosphatidylethanolamine; PC - phosphatidylcholine; PE - phosphatidylethanolamine; TAG - triacylglycerol.

METABOLITE	CLASS	Experiment 1					Experiment 2				
		c1	c2	c3	c4	c5	c1	c2	c3	c4	c5
Pipecolic acid	Amino acids and related	1.12	1.51	2.06	7.38	44.41	1.43	1.35	1.91	5.05	52.07
Tyrosine (GC)	Amino acids and related	1.21	1.45	1.87	11.73	2.05	1.06	1.20	1.37	8.37	2.65
Tyrosine (LC)	Amino acids and related	1.30	1.62	1.79	4.35	1.77	1.02	1.02	1.09	3.06	2.02
LPC (C18:2) (LC _n)	Lysoglycerophospholipids	1.22	1.01	1.43	2.02	2.79	1.13	1.14	1.29	1.22	2.27
Unknown polar (838000430)	Unknown	1.12	0.95	1.42	1.17	0.86	1.05	1.12	1.24	1.01	1.29
LPC (C18:2) (LC _n)	Lysoglycerophospholipids	1.15	1.06	1.24	1.64	2.24	1.28	1.08	1.40	1.30	2.39
LPC (C16:1)	Lysoglycerophospholipids	1.11	1.06	1.29	1.49	1.65	1.16	1.13	1.35	1.10	1.81
LPC (C18:3)	Lysoglycerophospholipids	1.10	1.04	1.26	1.64	1.84	1.28	1.02	1.29	1.38	2.11
Unknown polar (838000431)	Unknown	1.30	1.22	1.26	1.19	1.33	1.30	1.01	1.13	1.21	2.00
LPC (C20:5)	Lysoglycerophospholipids	1.12	1.09	1.24	1.23	0.42	0.96	0.88	0.97	0.92	0.40
LPC (C22:5)	Lysoglycerophospholipids	1.22	1.16	1.23	1.66	1.78	1.12	1.06	1.31	1.18	1.77
LPC (C22:4)	Lysoglycerophospholipids	1.09	1.02	1.21	1.56	1.85	1.12	1.09	1.17	1.12	1.96
LPC (C20:4)	Lysoglycerophospholipids	1.13	1.11	1.20	1.18	0.53	0.96	0.91	0.98	0.88	0.52
LPE (C18:2)	Lysoglycerophospholipids	1.00	1.02	1.19	1.14	1.48	1.00	1.14	1.09	0.88	1.28
LPC (C17:0)	Lysoglycerophospholipids	1.11	1.06	1.19	1.29	1.18	1.09	1.03	1.17	1.16	1.32
LPC (C22:6)	Lysoglycerophospholipids	1.09	1.05	1.17	1.45	1.51	1.07	1.02	1.10	1.07	1.13
LPE (C22:6)	Lysoglycerophospholipids	1.02	1.06	1.14	1.15	0.74	1.02	0.97	1.09	0.92	0.65
LPC (C18:1)	Lysoglycerophospholipids	1.10	1.08	1.13	1.46	1.76	1.23	1.14	1.31	1.14	1.68
Ceramide (d18:1,C23:0)	Sphingolipids	1.04	1.12	1.15	1.10	0.95	1.05	1.13	1.13	0.94	1.18
TAG (C18:1,C18:2,C18:3) (additional: TAG (C16:0,C18:1,C20:5), TAG (C16:0,C18:2,C20:4))	Acylglycerols	0.93	1.00	1.04	0.99	1.04	1.01	0.98	1.11	0.98	1.19
LPC (C20:3)	Lysoglycerophospholipids	1.21	1.07	1.10	1.48	1.64	1.29	1.12	1.33	1.10	2.05
myo-Inositol	Carbohydrates and related	0.96	1.00	1.10	1.27	1.23	1.00	1.04	1.05	1.28	1.33
Unknown lipid (848000204)	Unknown	1.08	0.97	1.07	1.10	1.11	1.03	0.99	0.91	1.03	1.26
PC (C36:3)	Glycerophospholipids	1.14	1.02	1.04	1.14	1.21	1.06	1.05	1.06	1.05	1.22
PE (C40:6)	Glycerophospholipids	1.00	0.99	0.99	1.00	0.97	1.00	1.01	0.99	1.00	1.00
PC (C32:0)	Glycerophospholipids	0.95	1.02	0.99	0.92	0.67	0.99	0.98	0.95	0.93	0.83
dihomo-gamma-Linolenic acid (C20:cis[8,11,14]3)	Fatty acids and related	0.88	0.99	0.94	0.94	0.85	1.04	1.00	1.11	0.97	0.96
Ceramide (d18:1,C20:0)	Sphingolipids	0.98	1.09	1.05	0.92	1.29	1.00	0.97	0.94	0.86	0.90
PE (C34:1)	Glycerophospholipids	0.90	1.04	0.93	0.89	0.92	0.99	0.95	1.02	0.90	0.93
PC (C36:4)	Glycerophospholipids	1.01	1.00	0.93	0.96	0.88	0.93	0.99	0.92	0.93	0.94
Choline	Energy metabolism and related	1.02	1.08	1.05	0.96	0.88	0.96	0.97	0.92	0.88	0.78
PE (C32:0)	Glycerophospholipids	0.85	0.95	0.91	0.77	0.47	0.96	0.95	0.92	0.81	0.43
Histidine	Amino acids and related	0.81	0.96	0.90	0.71	1.11	0.89	0.92	0.78	0.72	1.29
Asparagine (LC)	Amino acids and related	0.85	0.93	0.90	0.77	0.36	1.00	0.97	0.90	0.75	0.47
Taurine (LC)	Amino acids and related	0.90	0.97	0.91	0.77	0.56	0.91	0.92	0.89	0.93	0.82
2'-Deoxycytidine	Nucleobases and related	1.10	1.15	1.18	0.75	3.17	1.07	1.29	0.85	0.77	3.11
Glutamine (LC)	Amino acids and related	0.94	1.01	0.84	0.71	0.24	0.96	1.03	1.01	0.75	0.45
Phenylalanine (LC _n)	Amino acids and related	0.95	1.08	0.93	0.92	1.38	0.96	0.76	0.81	0.64	1.21
Unknown polar (878000055)	Unknown	1.04	1.04	1.09	0.90	0.56	0.97	0.83	0.80	0.77	0.57
Isoleucine (additional: Leucine)	Amino acids and related	0.97	0.94	0.95	0.75	0.49	0.97	0.83	0.79	0.67	0.54
Biliverdin	Miscellaneous	1.12	1.06	1.36	1.13	1.42	0.85	0.83	0.78	1.01	2.54
Nicotinamide	Vitamins, cofactors and related	1.07	1.05	1.04	0.98	2.11	1.31	0.99	0.77	0.93	0.70
N-Acetylaspartate	Amino acids and related	0.91	0.98	0.95	0.87	0.38	0.86	0.79	0.77	0.90	0.58
Methionine sulfoxide	Amino acids and related	0.98	0.91	0.93	0.77	0.31	1.00	0.92	0.74	0.42	0.35
Aspartate	Amino acids and related	0.73	0.77	0.71	0.57	0.24	1.06	0.94	0.88	0.85	0.41
Methionine (LC)	Amino acids and related	0.94	1.02	0.95	0.77	0.23	0.96	0.78	0.65	0.54	0.29
Fructose-6-phosphate	Energy metabolism and related	0.92	1.29	1.04	1.01	0.08	1.02	0.95	0.29	0.70	0.08

0.5	2.0
Wilcoxon signed-rank test	$p < 0.05$
	$0.05 \leq p \leq 0.1$
	$p > 0.1$

Since the previous analyses showed that some metabolite classes were more affected, the effects were also evaluated at the class level. In total, almost 20% of the measured metabolites were significantly altered at concentration c3 (Fig. 6). The class of lysoglycerophospholipids stood out with 46% of significantly changed metabolites. Further classes with a high proportion of significantly changed metabolites were the amino acids and related (30%), and carbohydrates and related (25%). Of all other classes, less than 20% of the measured metabolites were significantly altered.

3.5. Affected amino acid-related pathways show concentration-dependent response

To obtain mechanistic information, metabolite changes were examined in the context of the metabolic pathway map from KEGG. All significantly affected pathways at c3 were considered, and their progression in further concentrations. For most pathways, a concentration-response relationship with respect to increasing significances was observed, peaking at c5 (15/21) or c4 (5/21), respectively (Fig. 7). Overall, the proportion of amino acid-related pathways affected was about 60%.

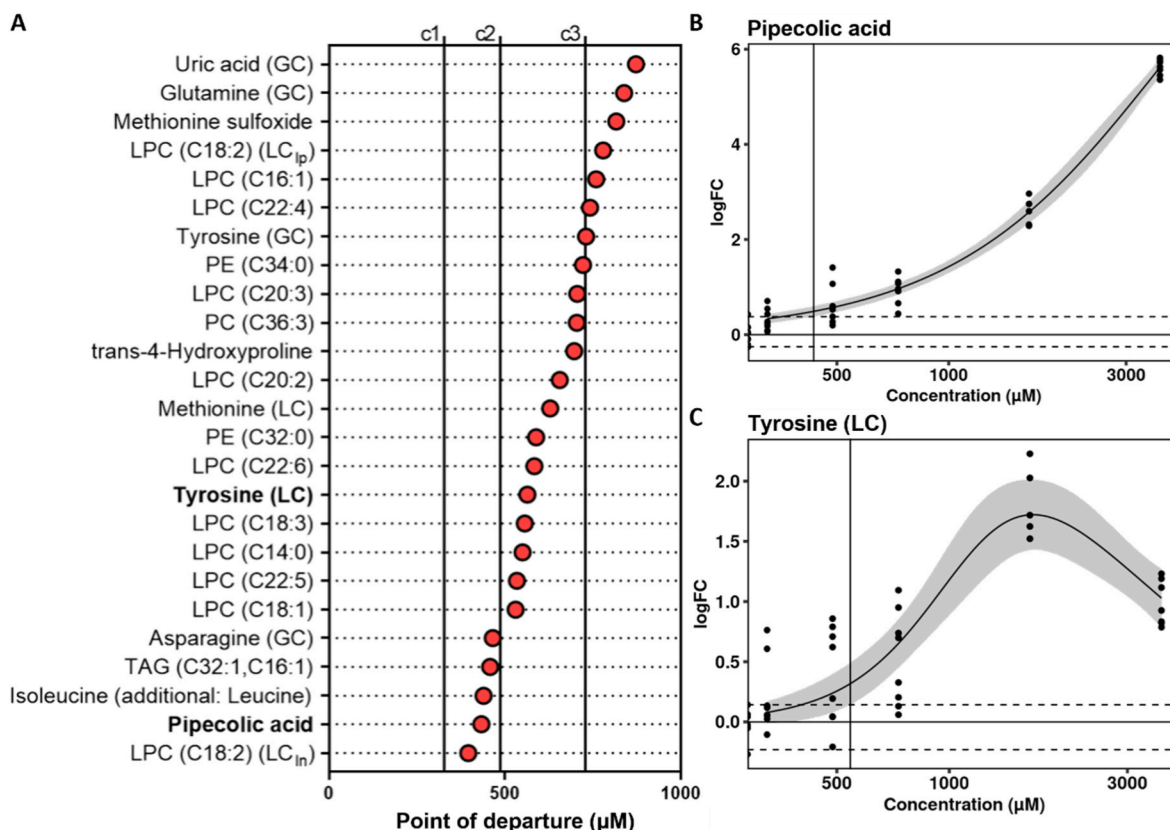


Fig. 5. Point of departures (PoD) for the most sensitive metabolites after exposure of zebrafish embryos to PTU. For each metabolite, the concentration-dependent response was modeled. The PoD is the concentration at which the effect exceeds control variability. A) The 25 most sensitive metabolites are shown in ascending order. A low PoD indicates a high sensitivity. B) and C) Exemplary curve fits for pipecolic acid (B) and tyrosine (C) are shown and highlighted in (A) for reference. The PoD is indicated with a solid vertical line. It marks the concentration at which the confidence interval of the curve (grey shaded area) intersects the control variability (dashed lines). FC - fold change; GC - gas chromatography; LC - liquid chromatography; LPC - lysophosphatidylcholine; PC - phosphatidylcholine; PE - phosphatidylethanolamine; TAG - triacylglycerol.

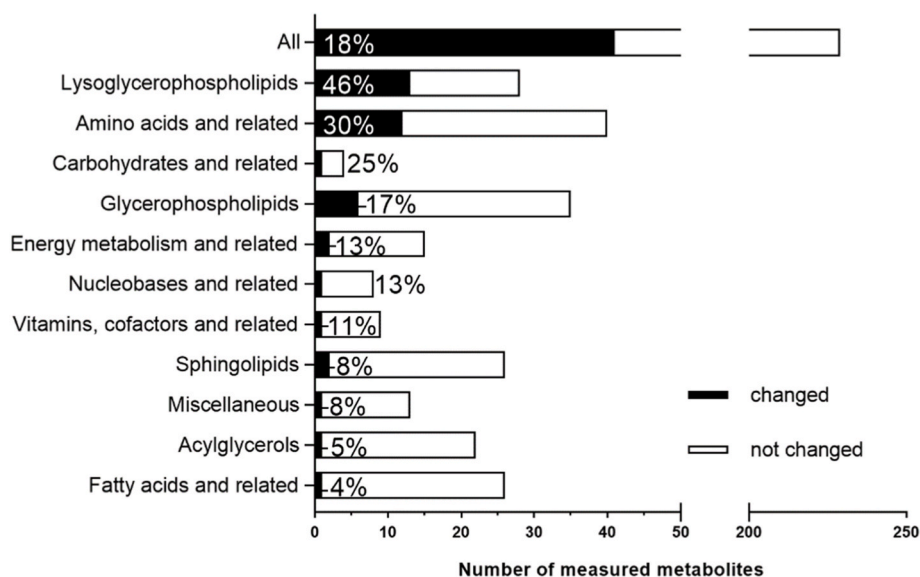


Fig. 6. Proportion of significantly changed versus unchanged metabolites at concentration c3 among different metabolite classes. To determine the distribution of changes among various metabolite classes, 230 annotated unique metabolites (out of 249) were considered. For each class, the length of the bar indicates the total number of metabolites and the shaded region the percentage of significantly ($p \leq 0.1$) changed ones. Overall, 41 metabolites accounting for 18% were significantly changed in at least one experiment at c3. From the class of signal substances and related, no metabolite was significantly changed at c3.

The impact value provides information about the importance of the measured metabolites, it is a measure for their interconnectivity in the pathway. The highest achievable impact value of 1 was reached exclusively by the ‘Phenylalanine, tyrosine and tryptophan biosynthesis’. This pathway includes two measured metabolites, namely phenylalanine and

tyrosine. Since these are directly linked and thus highly dependent, the pathway achieved the highest impact value. Beyond that, only ‘Alanine, aspartate and glutamate metabolism’ (impact of 0.76), ‘Arginine biosynthesis’ (impact of 0.60), ‘Riboflavin metabolism’ (impact of 0.5), and ‘Arginine and proline metabolism’ (impact of 0.55) reached an

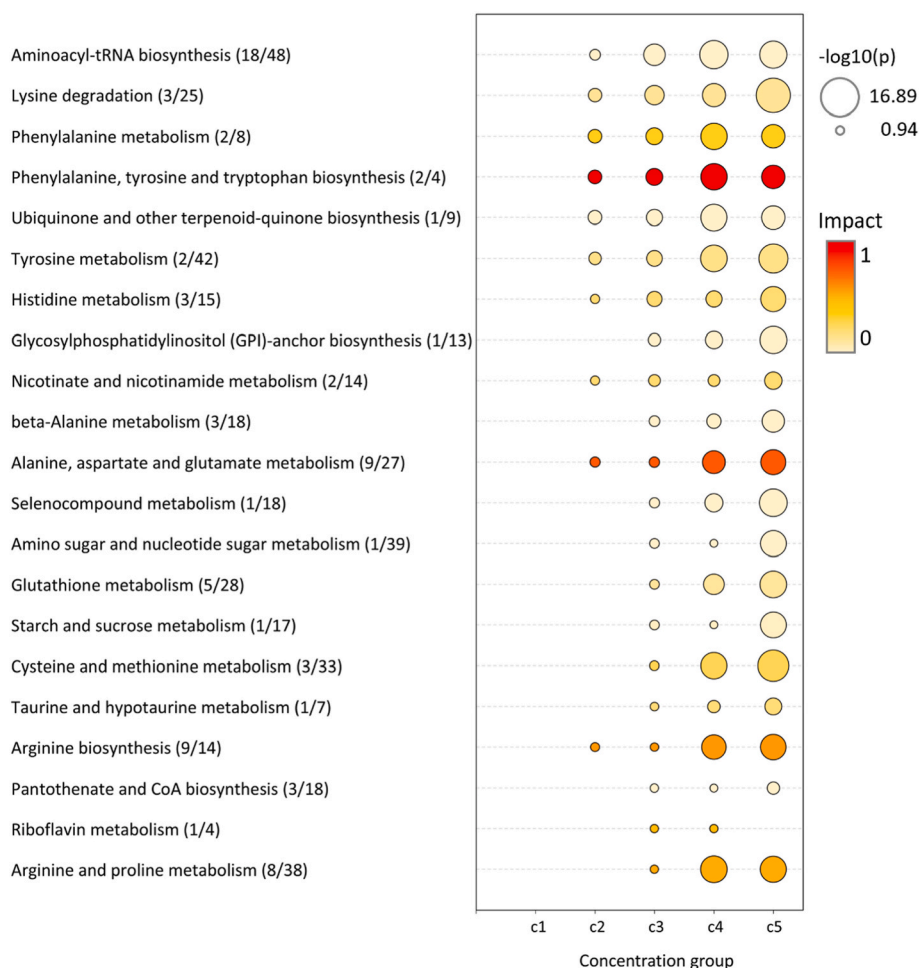


Fig. 7. Significantly affected pathways based on metabolic response to PTU treatment. Using the web-based tool MetaboAnalyst 5.0 [46] the concentration-dependent influence of PTU treatment on endogenous metabolic pathways of zebrafish embryos was investigated. A threshold of FDR <0.25 was applied to filter out the significantly affected pathways. Only pathways significantly affected at concentration c3 were considered. The figure is ordered by $-\log_{10}(p)$ -values of c3. The circle size signifies the confidence on the pathway being affected by the treatment. The impact value is indicated by the color scheme and is a measure for the importance of the measured metabolites for the pathway (details in section 2.11). Numbers in parentheses indicate how many metabolites were measured out of the total number of the metabolites in the pathway. Values and exemplary pathways can be found in the supplementary (Table S4 and Fig. S3).

impact value greater than 0.5.

4. Discussion

The objective of the study was to investigate the ability of the zebrafish embryo metabolome to indicate developmental toxicity. For this, the robustness of metabolic effects in different batches of zebrafish was tested in terms of their reproducibility. The metabolic effect pattern was compared for plausibility with relevant literature and related to the morphological changes. In elaborating the effects associated with the mode of action of PTU, special emphasis was paid to the distinction between the presumably specific and more general toxic effects by regarding concentration-dependent responses.

4.1. Effects of PTU exposure on swim bladder and eye development

The most sensitive morphological endpoint was swim bladder inflation with an EC_{50} of 124 μ M. Thus, this endpoint was even more sensitive than any measured metabolite, as the lowest PoD was determined at 396 μ M for LPC (C18:2) (LC_{10}). The zebrafish swim bladder consists of two chambers. While the posterior chamber inflates between 96 and 144 hpf, inflation of the anterior chamber occurs earliest around 21 days post fertilization [48,49]. A previously described adverse outcome pathway (AOP) network linked impaired anterior swim bladder inflation to thyroid disruption and developmental toxicity [50–52], but due to the duration of treatment in this study, only the development of the posterior swim bladder was considered. Earlier studies have shown that this endpoint is in general sensitive to a variety of chemicals [37], indicating that the responses observed here might not

be specific to PTU, but more related to a general developmental delay. In addition, controversial results on swim bladder inflation with other TPO inhibitors are existing: For methimazole, two studies showed reduced inflation [33,53] while other studies did not observe an effect [54,55]. For 2-mercaptobenzothiazole, no effects on the swim bladder were observed [54,56,57]. Since the mechanism of posterior swim bladder development is unclear, there is weak evidence that this phenotype is specifically linked to reduced thyroid hormone levels.

Besides the impairment of the swim bladder, our data indicated morphological alterations for the size of the eyes, body, and head. Our results are consistent with previous studies in which thyroid disruption was frequently linked to ocular morphological alterations and retardation [32,33,58,59]. In particular, effects on eye development were considered as highly associated with TPO inhibition in fish and have been included as an endpoint of an AOP lately [60]. Decreased eye size was a more sensitive endpoint than decreased whole organism length in this study, but its expression must also be considered in the context of general retardation.

4.2. Effects of PTU on the metabolome and their relation to developmental toxicity

Addressing the utility of the zebrafish embryo metabolome to reveal molecular changes related to developmental toxicity, two main aspects were considered: reproducibility of the method and relationship of the findings with the mode of action of PTU.

The metabolome data from two experiments, each including five concentrations demonstrated reproducibility based on the overall response as shown in the PCA, the PCA-derived PoDs, and for individual

metabolite changes. Additionally, the concentration-dependent effects illustrated the reliability of the experimental setup.

To elicit the metabolic effects that reflect the mode of action of PTU and developmental toxicity, we applied two approaches based on different statistical methods. Both aimed at filtering out the specific effects and excluding secondary effects. Secondary effects are supposed to occur both at high concentrations in the sense of general cytotoxicity and at lower concentrations in terms of nonspecific adaptive changes. To achieve the separation of specific and nonspecific effects, one approach focused particularly on c3, the concentration group, which depicts the beginning of an overall deviation in the metabolome from the controls. The second approach inspected the concentration-dependent response of each metabolite. In this study, both approaches have shown high overlap when comparing the metabolites returned. This can potentially be attributed to the selection of test concentrations, which were chosen to span the entire range from adaptive to specific to cytotoxic effects. Although concentrations greater than 1000 μM are often not considered relevant in risk assessment, it may be beneficial to include higher concentrations that allow modeling of a concentration-response curve and determination of the PoD. In the study presented, we have not yet exploited the full potential of the PoD. It was mainly used qualitatively, e.g., to obtain a sensitivity ranking of the metabolites. Also, a quantitative use is conceivable to derive a no-effect level that could feed into human or ecological risk assessment.

Focusing on the specific metabolite changes, strongly increased levels and a low PoD were observed for pipercolic acid and tyrosine. Pipercolic acid is an intermediate in the lysine degradation pathway [61]. The formation of pipercolic acid from Δ^1 -piperideine-2-carboxylate is catalyzed by CRYM (μ -crystallin), which is regulated by binding of thyroid hormones [62–64]. It was shown that the binding of T3 leads to an inhibition of the enzyme. This demonstrates the vulnerability of the pipercolic acid pathway to thyroid disrupting compounds. Rehberger et al. [65] have found a significant decrease in follicular T3 after treating zebrafish embryos with PTU. We hypothesize that a decrease in T3 affects the regulation of CRYM which results in an increase of pipercolic acid.

In contrast to pipercolic acid, tyrosine is directly related to the thyroid hormone synthesis. Tyrosine is the biochemical precursor of the thyroid hormones, formed from the coupling of iodinated tyrosine residues of thyroglobulin. By inhibiting the enzyme TPO, which catalyzes this step, a decrease in T3 and T4 was reported [59,65,66] while the expression of thyroglobulin was induced [35] potentially as a feedback loop response to compensate for reduced hormone levels. Under physiological conditions, the feedback loop detects low hormone levels and responds by stimulating hormone production [67]. Possibly, elevated tyrosine levels may also be the result of accumulation due to the block of thyroid hormone synthesis. However, tyrosine is not only a precursor of thyroid hormones but also of other bioactive molecules, such as dopamine or melanin. Hence it is conceivable that the increase in tyrosine may not solely be due to the impairment of the thyroid hormone signaling pathway.

Although the lysoglycerophospholipids were only slightly increased, the observation that half of them were significantly altered at c3 and some lysophosphatidylcholines (LPCs) were even among the top 25 PoDs, suggests a relevant effect of PTU treatment on this class of metabolites. During embryogenesis, the yolk sac serves as a reservoir for nutrient lipids, and for a long time it was mainly considered as such [68]. In 2016, Fraher et al. [69] published a study which analyzed lipid species composition of the yolk sac at different time points during zebrafish embryonic and early larval development. Contrary to initial assumptions, they found that the yolk is metabolically active. Furthermore, they characterized the physiological state of the yolk sac, which provides a good basis for comparison. From 0 to 120 hpf all lysoglycerophospholipids like e.g., the LPCs showed a distinct decrease except for the lysophosphatidylethanolamines. In contrast, we found that all significantly changed LPCs at c3 were increased. Similarly, Fraher et al.

[69] described an increase of LPCs after treating zebrafish with a PPAR γ receptor inhibitor. There is growing evidence that lysoglycerophospholipids have important physiological functions [70]. LPCs were recognized as a source of neuronal membrane components [71]. Furthermore, it was shown that LPCs can overcome the blood brain barrier using Mfsd2a transporters. In turn, a lack of the Mfsd2a transporter was associated with increased LPCs and brain defects like e.g., microcephaly [72,73]. Since this mechanism is conserved from fish to humans, it is possible that elevated LPCs could be related to impaired brain development, which in turn could be associated with the known impact of thyroid hormones on the development of the nervous system. The presence of potential developmental neurotoxicity is further supported by the observed reduced eye size and craniofacial anomalies.

Our data contain further evidence suggestive of impaired neurodevelopment. Methionine was strongly decreased at c3 and showed a concentration-dependent response with a low PoD. In studies using rat embryos cultured *in vitro*, defects in neural tube closure were associated with methionine deficiency in the culture medium [74,75]. Likewise, the lysine degradation pathway, whose intermediate pipercolic acid was measured to be highly elevated, was described in the context of impaired neuronal development [76,77].

Beyond individual metabolite or class changes, the orchestration of multiple metabolites in a pathway may be disrupted by a substance exposure. To reveal disrupted pathways, a metabolic pathway analysis was conducted, which contextualizes individual metabolite changes. With 12 metabolite classes and 50 subclasses, the measured metabolome covered a large part of the endogenous metabolic pathway map. However, the diversity of measured lipid species was underrepresented in the database, therefore only 109 metabolites could be assigned a unique metabolite ID. Similar to the directional switch observed in Table 1, several pathways with a peaking significance at c4 also hinted at a comprehensive change in the whole metabolome between c4 and c5. The biological system seems to reach a tipping point between c4 and c5, after which primarily general cytotoxic effects may be present. This is supported by the mortality concentrations. While c5 correlates with an LC₂₅, which is associated with overt toxicity, c4 corresponds to an LC₁₀, and equivalent mortality would be tolerated even in controls according to TG 236 [34].

Among the pathways that peaked at c4, the phenylalanine, tyrosine and tryptophan biosynthesis achieved the highest impact value. The two changed metabolites in this pathway were phenylalanine and tyrosine. While tyrosine was strongly increased, phenylalanine was slightly decreased. Taking into consideration the whole metabolic map, this effect marks a molecular target of PTU, which is the inhibition of TPO. When viewing the entire KEGG metabolic pathway map, only tyrosine was measured as a direct neighbor of this event; phenylalanine, in turn, is the precursor of tyrosine. The decrease in phenylalanine could be explained by compensatory mechanisms for high tyrosine concentrations. The identification of a molecular target of PTU as a result of the pathway analysis highlights the value of integrating a contextual analysis. This could become especially important for analyzing compounds whose mode of action is unclear.

4.3. Conclusions

This study has shown that the combination of metabolome and morphology assessment in zebrafish embryo is a robust system that reveals specific effects related to the mode of action of PTU or developmental toxicity in general. Effects on tyrosine, pipercolic acid, and the phenylalanine, tyrosine and tryptophan biosynthesis could be tied to PTU treatment and seem to be indicative of changes in the thyroid hormone system. This and other changes in metabolites such as increased LPCs and decreased methionine also suggested neurodevelopmental toxicity. The presence of neurodevelopmental toxicity was further supported by the decreased eye size, which was the most eminent morphological effect observed. The demonstration of

reproducible, concentration-dependent, and plausible effects underscores the utility of metabolomics for identifying developmental toxicity in zebrafish embryo. Revealing the mechanism of toxicity represents a critical step in overcoming limitations in the transferability of morphological endpoints to humans. The major signaling pathways of embryogenesis are conserved in vertebrates, which was supported by the present study. Subsequent studies need to examine different compound classes to provide further evidence for the relevance and specificity of metabolome response. A prospective challenge may also be an increase in the coverage of metabolic pathways, which is limited in a targeted approach.

Author statement

Conceptualization: B. Flick, S. Henkes, S. Scholz, W. Busch, H. Kamp; Methodology: P. Driemert, S. Scholz, W. Busch, P. Wilhelmi, V. Giri, V. Haake; Investigation: P. Wilhelmi, V. Giri, F.M. Zickgraf, W. Busch, S. Scholz, B. Flick; Data analysis: P. Wilhelmi, V. Giri, P. Michaelis, V. Haake, S. Scholz; Writing original draft: P. Wilhelmi; Editing: V. Giri, F. M. Zickgraf, S. Scholz, W. Busch; Project management and Supervision: F.M. Zickgraf, S. Henkes, S. Scholz, B. Birk, B. Flick; Funding acquisition and Resources: R. Landsiedel, D. Funk-Weyer, B. Flick, S. Scholz, H. Kamp; Review: M. Barenys, B. Birk, H. Kamp, B. Flick, R. Landsiedel, D. Funk-Weyer.

Funding information

The experimental work was funded by BASF SE, Key Technology Capability (KTC) building *Alternative Toxicological Methods*, by the Earth and Environment Research Program of the Helmholtz Association (Topic 9) and supported by the major infrastructure initiative CITEPro (Chemicals in the Terrestrial Environment Profiler) at the UFZ. The data evaluation was supported by the German Ministry of Education and Research to the project ZF-AOP (BMBF Förderkennzeichen 031L0232 A/B). Zebrafish ontology terms or the corresponding feature translation table (Table S1), respectively, were established as part of the EU project PrecisionTox.

Declaration of competing interest

The authors declare that they have no known competing financial interests or personal relationships that could have appeared to influence the work reported in this paper.

Data availability

Data will be made available on request.

Acknowledgments

The authors thank Bennard van Ravenzwaay for the conceptual discussions and for editing the manuscript, and Philippe Rocce-Sera (University of Oxford) and Nils Klüver (UFZ) for advice with zebrafish ontologies.

Appendix A. Supplementary data

Supplementary data to this article can be found online at <https://doi.org/10.1016/j.cbi.2023.110565>.

References

- [1] Regulation (EC) No 1907/2006, Registration, evaluation, authorisation and restriction of chemicals (REACH). <https://osha.europa.eu/>. (Accessed 19 January 2023).
- [2] Directive 2001/83/EC, EudraLex-Volume1-Pharmaceutical legislation for medicinal products for human use. <https://health.ec.europa.eu/>. (Accessed 13 February 2023).
- [3] G. Koren, A. Ornoy, The role of the placenta in drug transport and fetal drug exposure, *Expet Rev. Clin. Pharmacol.* 11 (4) (2018) 373–385, <https://doi.org/10.1080/17512433.2018.1425615>.
- [4] OECD, "Test No. 414: prenatal developmental toxicity study,". <https://www.oecd-ilibrary.org/>, 2018. (Accessed 20 August 2022).
- [5] L. Wise, The ICH S5(R2) guideline for the testing of medicinal agents, *Methods Mol. Biol.* 947 (2013) 1–11, https://doi.org/10.1007/978-1-62703-131-8_1.
- [6] R. Landsiedel, et al., The evolution of regulatory toxicology: where is the gardener? *Altern. Lab. Anim.* 50 (4) (2022) 255–262, <https://doi.org/10.1177/02611929221107617>.
- [7] L. Meigs, et al., Animal testing and its alternatives - the most important omics is economics, *ALTEX* 35 (3) (2018) 275–305, <https://doi.org/10.14573/altex.1807041>.
- [8] S. Scholz, et al., A European perspective on alternatives to animal testing for environmental hazard identification and risk assessment, *Regul. Toxicol. Pharmacol.* 67 (3) (2013) 506–530, <https://doi.org/10.1016/j.yrtph.2013.10.003>.
- [9] C. Rovida, T. Hartung, Re-evaluation of animal numbers and costs for in vivo tests to accomplish REACH legislation requirements for chemicals - a report by the transatlantic think tank for toxicology (t4), *Altex* 26 (3) (2009) 187–208, <https://doi.org/10.14573/altex.2009.3.187>.
- [10] K.S. Hougaard, Next generation reproductive and developmental toxicology: crosstalk into the future, *Front. Toxicol., Specialty Grand Challenge 3* (2021), <https://doi.org/10.3389/ftox.2021.652571>.
- [11] M. Barenys, et al., Developmental exposure to MDMA (ecstasy) in zebrafish embryos reproduces the neurotoxicity adverse outcome 'lower motor activity' described in humans, *Neurotoxicology* 88 (2022) 116–123, <https://doi.org/10.1016/j.neuro.2021.11.001>.
- [12] I.G.E. Gebuijs, et al., The Anti-epileptic Drug Valproic Acid Causes Malformations in the Developing Craniofacial Skeleton of Zebrafish Larvae, vol. 163, *Mechanisms of Development*, 2020, <https://doi.org/10.1016/j.mod.2020.103632>. Art no. 103632.
- [13] M. Driessen, et al., Exploring the zebrafish embryo as an alternative model for the evaluation of liver toxicity by histopathology and expression profiling, *Arch. Toxicol.* 87 (5) (2013) 807–823, <https://doi.org/10.1007/s00204-013-1039-z>.
- [14] U. Strähle, et al., Zebrafish embryos as an alternative to animal experiments—a commentary on the definition of the onset of protected life stages in animal welfare regulations, *Reprod. Toxicol.* 33 (2) (2012) 128–132, <https://doi.org/10.1016/j.reprotox.2011.06.121>.
- [15] EU Directive, "63/EU of the European Parliament and of the Council of 22 September 2010 on the protection of animals used for scientific purposes,". *Off. J. Eur. Union* 276 (2010) 33–79.
- [16] S. Hoffmann, et al., A systematic Review to compare chemical hazard predictions of the zebrafish embryotoxicity test with mammalian prenatal developmental toxicity, *Toxicol. Sci.* 183 (1) (2021) 14–35, <https://doi.org/10.1093/toxsci/kfab072>.
- [17] Y. Nishimura, et al., Using zebrafish in systems toxicology for developmental toxicity testing, *Congenital. Anom.* 56 (1) (2016) 18–27, <https://doi.org/10.1111/cga.12142>.
- [18] J.S. Ball, et al., Fishing for teratogens: a consortium effort for a harmonized zebrafish developmental toxicology assay, *Toxicol. Sci.* 139 (1) (2014) 210–219, <https://doi.org/10.1093/toxsci/kfu017>.
- [19] C.H. Johnson, J. Ivanisevic, G. Siuzdak, Metabolomics: beyond biomarkers and towards mechanisms, *Nat. Rev. Mol. Cell Biol.* 17 (7) (2016) 451–459, <https://doi.org/10.1038/nrm.2016.25>.
- [20] S. Ramirez-Hincapie, et al., Influence of pregnancy and non-fasting conditions on the plasma metabolome in a rat prenatal toxicity study, *Arch. Toxicol.* 95 (9) (2021) 2941–2959, <https://doi.org/10.1007/s00204-021-03105-0>.
- [21] W. Mattes, et al., Detection of hepatotoxicity potential with metabolite profiling (metabolomics) of rat plasma, *Toxicol. Lett.* 230 (3) (2014) 467–478, <https://doi.org/10.1016/j.toxlet.2014.07.021>.
- [22] J. Keller, et al., Added value of plasma metabolomics to describe maternal effects in rat maternal and prenatal toxicity studies, *Toxicol. Lett.* 301 (2019) 42–52, <https://doi.org/10.1016/j.toxlet.2018.10.032>.
- [23] T. Ramirez, et al., Prediction of liver toxicity and mode of action using metabolomics in vitro in HepG2 cells, *Arch. Toxicol.* 92 (2) (2018) 893–906, <https://doi.org/10.1007/s00204-017-2079-6>.
- [24] J.M. Davis, et al., Metabolomics for informing adverse outcome pathways: androgen receptor activation and the pharmaceutical spironolactone, *Aquat. Toxicol.* 184 (2017) 103–115, <https://doi.org/10.1016/j.aquatox.2017.01.001>.
- [25] W. Liu, et al., Developmental toxicity of TCBP on the nervous and cardiovascular systems of zebrafish (*Danio rerio*): a combination of transcriptomic and metabolomics, *J. Environ. Sci.* 127 (2023) 197–209, <https://doi.org/10.1016/j.jes.2022.04.022>.
- [26] DrugBank, Propylthiouracil. <https://go.drugbank.com/drugs/DB00550>. (Accessed 12 July 2022).
- [27] B. Davidson, et al., The irreversible inactivation of thyroid peroxidase by methylmercaptoimidazole, thiouracil, and propylthiouracil in vitro and its relationship to in vivo findings, *Endocrinology* 103 (3) (1978) 871–882, <https://doi.org/10.1210/endo-103-3-871>.
- [28] A.G. Weber, et al., A new approach method to study thyroid hormone disruption: optimization and standardization of an assay to assess the inhibition of DIO1 enzyme in human liver microsomes, *Appl. In Vitro Toxicol.* 8 (3) (2022) 67–82, <https://doi.org/10.1089/aivt.2022.0010>.

- [29] T. Nogimori, et al., A new class of propylthiouracil analogs: comparison of 5'-deiodinase inhibition and antithyroid activity, *Endocrinology* 118 (4) (1986) 1598–1605, <https://doi.org/10.1210/endo-118-4-1598>.
- [30] V.C. Benavides, et al., Propylthiouracil is teratogenic in murine embryos, *PLoS One* 7 (4) (2012), e35213, <https://doi.org/10.1371/journal.pone.0035213>.
- [31] M. Axelstad, et al., Developmental neurotoxicity of Propylthiouracil (PTU) in rats: relationship between transient hypothyroxinemia during development and long-lasting behavioural and functional changes, *Toxicol. Appl. Pharmacol.* 232 (1) (2008) 1–13, <https://doi.org/10.1016/j.taap.2008.05.020>.
- [32] L. Baumann, et al., Thyroid disruption in zebrafish (*Danio rerio*) larvae: different molecular response patterns lead to impaired eye development and visual functions, *Aquat. Toxicol.* 172 (2016) 44–55, <https://doi.org/10.1016/j.aquatox.2015.12.015>.
- [33] B. Jomaa, et al., Developmental toxicity of thyroid-active compounds in a zebrafish embryotoxicity test, *Altox* 31 (3) (2014) 303–317, <https://doi.org/10.14573/altox.1402011>.
- [34] OECD, "Test No. 236: fish embryo acute toxicity (FET) test,". <https://www.oecd-ilibrary.org/>, 2013. (Accessed 20 August 2022).
- [35] S. Jarque, et al., An automated screening method for detecting compounds with goitrogenic activity using transgenic zebrafish embryos, *PLoS One* 13 (8) (2018), e0203087, <https://doi.org/10.1371/journal.pone.0203087>.
- [36] E. Teixidó, et al., Automated morphological feature assessment for zebrafish embryo developmental toxicity screens, *Toxicol. Sci.* 167 (2) (2019) 438–449, <https://doi.org/10.1093/toxsci/kfy250>.
- [37] E. Teixidó, et al., Grouping of chemicals into mode of action classes by automated effect pattern analysis using the zebrafish embryo toxicity test, *Arch. Toxicol.* 96 (5) (2022) 1353–1369, <https://doi.org/10.1007/s00204-022-03253-x>.
- [38] Z. Xiang, et al., Ontobee: a linked data server and browser for ontology terms, in: *CEUR Workshop Proceedings*, vol. 833, 2011, pp. 279–281 [Online], <https://ceur-ws.org/Vol-833/paper48.pdf>. (Accessed 14 February 2023).
- [39] U. Roessner, et al., Technical advance: simultaneous analysis of metabolites in potato tuber by gas chromatography-mass spectrometry, *Plant J.* 23 (1) (2000) 131–142, <https://doi.org/10.1046/j.1365-313x.2000.00774.x>.
- [40] R Core Team, "R: A Language and Environment for Statistical Computing, R Foundation for Statistical Computing, Vienna, Austria, 2022. <https://www.R-project.org/>. (Accessed 2 January 2023).
- [41] T. Hastie, et al., "Impute: Imputation for Microarray Data. R Package Version 1.54.0," 2020, <https://doi.org/10.18129/B9.bioc.impute>.
- [42] H. Wickham, *ggplot2: Elegant Graphics for Data Analysis*, Springer-Verlag, New York, 2016, ISBN 978-3-319-24277-4, pp. 189–201.
- [43] C. Ritz, et al., Dose-response analysis using R, *PLoS One* 10 (12) (2015), e0146021, <https://doi.org/10.1371/journal.pone.0146021>.
- [44] B. Birk, et al., Use of in vitro metabolomics in NRK cells to help predicting nephrotoxicity and differentiating the MoA of nephrotoxicants, *Toxicol. Lett.* 353 (2021) 43–59, <https://doi.org/10.1016/j.toxlet.2021.09.011>.
- [45] Z. Pang, et al., MetaboAnalyst 5.0: narrowing the gap between raw spectra and functional insights, *Nucleic Acids Res.* 49 (W1) (2021) W388–W396, <https://doi.org/10.1093/nar/gkab382>.
- [46] MetaboAnalyst. 5.0 - user-friendly, streamlined metabolomics data analysis. <https://www.metaboanalyst.ca>. (Accessed 23 November 2022).
- [47] J. Xia, D.S. Wishart, MetPA: a web-based metabolomics tool for pathway analysis and visualization, *Bioinformatics* 26 (18) (2010) 2342–2344, <https://doi.org/10.1093/bioinformatics/btq418>.
- [48] C.L. Winata, et al., Development of zebrafish swimbladder: the requirement of Hedgehog signaling in specification and organization of the three tissue layers, *Dev. Biol.* 331 (2) (2009) 222–236, <https://doi.org/10.1016/j.ydbio.2009.04.035>.
- [49] G.N. Robertson, et al., Development of the swimbladder and its innervation in the zebrafish, *Danio rerio*, *J. Morphol.* 268 (11) (2007) 967–985, <https://doi.org/10.1002/jmor.10558>.
- [50] D. Noyes Pamela, et al., Evaluating chemicals for thyroid disruption: opportunities and challenges with in vitro testing and adverse outcome pathway approaches, *Environ. Health Perspect.* 127 (9) (2019), 095001, <https://doi.org/10.1289/EHP5297>.
- [51] D. Knapen, et al., Toward an AOP network-based tiered testing strategy for the assessment of thyroid hormone disruption, *Environ. Sci. Technol.* 54 (14) (2020) 8491–8499, <https://doi.org/10.1021/acs.est.9b07205>.
- [52] M. Heijlen, et al., Knockdown of type 3 iodothyronine deiodinase severely perturbs both embryonic and early larval development in zebrafish, *Endocrinology* 155 (4) (2014) 1547–1559, <https://doi.org/10.1210/en.2013-1660>.
- [53] O.A. Elsalini, K.B. Rohr, Phenylthiourea disrupts thyroid function in developing zebrafish, *Dev. Gene. Evol.* 212 (12) (2003) 593–598, <https://doi.org/10.1007/s00427-002-0279-3>.
- [54] E. Stinckens, et al., Effect of thyroperoxidase and deiodinase inhibition on anterior swim bladder inflation in the zebrafish, *Environ. Sci. Technol.* 54 (10) (2020) 6213–6223, <https://doi.org/10.1021/acs.est.9b07204>.
- [55] Y.-W. Liu, W.-K. Chan, Thyroid hormones are important for embryonic to larval transitory phase in zebrafish, *Differentiation* 70 (1) (2002) 36–45, <https://doi.org/10.1046/j.1432-0436.2002.700104.x>.
- [56] E. Stinckens, et al., Impaired anterior swim bladder inflation following exposure to the thyroid peroxidase inhibitor 2-mercaptobenzothiazole part II: zebrafish, *Aquat. Toxicol.* 173 (2016) 204–217, <https://doi.org/10.1016/j.aquatox.2015.12.023>.
- [57] K.R. Nelson, et al., Impaired anterior swim bladder inflation following exposure to the thyroid peroxidase inhibitor 2-mercaptobenzothiazole part I: fathead minnow, *Aquat. Toxicol.* 173 (2016) 192–203, <https://doi.org/10.1016/j.aquatox.2015.12.024>.
- [58] Z. Li, D. Ptak, et al., Phenylthiourea specifically reduces zebrafish eye size, *PLoS One* 7 (6) (2012), e40132, <https://doi.org/10.1371/journal.pone.0040132>.
- [59] D. Raldúa, P.J. Babin, Simple, rapid zebrafish larva bioassay for assessing the potential of chemical pollutants and drugs to disrupt thyroid gland function, *Environ. Sci. Technol.* 43 (17) (2009) 6844–6850, <https://doi.org/10.1021/es9012454>.
- [60] L. Gözl, et al., AOP report: thyroperoxidase inhibition leading to altered visual function in fish via altered retinal layer structure, *Environ. Toxicol. Chem.* 41 (11) (2022) 2632–2648, <https://doi.org/10.1002/etc.5452>.
- [61] J. Leandro, S.M. Houten, The lysine degradation pathway: subcellular compartmentalization and enzyme deficiencies, *Mol. Genet. Metabol.* 131 (1–2) (2020) 14–22, <https://doi.org/10.1016/j.ymgme.2020.07.010>.
- [62] A. Hallen, J.F. Jamie, A.J. Cooper, Lysine metabolism in mammalian brain: an update on the importance of recent discoveries, *Amino Acids* 45 (6) (2013) 1249–1272, <https://doi.org/10.1007/s00726-013-1590-1>.
- [63] J.-i. Mori, et al., Nicotinamide adenine dinucleotide phosphate-dependent cytosolic T3 binding protein as a regulator for T3-mediated transactivation, *Endocrinology* 143 (4) (2002) 1538–1544, <https://doi.org/10.1210/endo.143.4.8736>.
- [64] A. Beslin, et al., Identification by photoaffinity labelling of a pyridine nucleotide-dependent tri-iodothyronine-binding protein in the cytosol of cultured astroglial cells, *Biochem. J.* 305 (Pt 3) (1995) 729–737, <https://doi.org/10.1042/bj3050729>.
- [65] K. Rehberger, et al., Intrafollicular thyroid hormone staining in whole-mount zebrafish (*Danio rerio*) embryos for the detection of thyroid hormone synthesis disruption, *Fish Physiol. Biochem.* 44 (3) (2018) 997–1010, <https://doi.org/10.1007/s10695-018-0488-y>.
- [66] B. Thienpont, et al., Zebrafish eleutheroembryos provide a suitable vertebrate model for screening chemicals that impair thyroid hormone synthesis, *Environ. Sci. Technol.* 45 (17) (2011) 7525–7532, <https://doi.org/10.1021/es202248h>.
- [67] J.W. Dietrich, G. Landgrafe, E.H. Fotiadou, TSH and thyrotropic agonists: Key actors in thyroid homeostasis, *J. Thyroid Res.* (2012), 351864, <https://doi.org/10.1155/2012/351864>.
- [68] M. Hölttä-Vuori, et al., Zebrafish: gaining popularity in lipid research, *Biochem. J.* Rev. 429 (2) (2010) 235–242, <https://doi.org/10.1042/BJ20100293>.
- [69] D. Fraher, et al., Zebrafish embryonic lipidomic analysis reveals that the yolk cell is metabolically active in processing lipid, *Cell Rep.* 14 (6) (2016) 1317–1329, <https://doi.org/10.1016/j.celrep.2016.01.016>.
- [70] S.T. Tan, et al., Emerging roles of lysophospholipids in health and disease, *Prog. Lipid Res., Rev.* 80 (2020), <https://doi.org/10.1016/j.plipres.2020.101068>. Art no. 101068.
- [71] L.N. Nguyen, et al., Mfsd2a is a transporter for the essential omega-3 fatty acid docosahexaenoic acid, *Nature* 509 (7501) (2014) 503–506, <https://doi.org/10.1038/nature13241>.
- [72] A. Guemez-Gamboa, et al., Inactivating mutations in MFSD2A, required for omega-3 fatty acid transport in brain, cause a lethal microcephaly syndrome, *Nat. Genet.* 47 (7) (2015) 809–813, <https://doi.org/10.1038/ng.3311>.
- [73] V. Alakbarzade, et al., A partially inactivating mutation in the sodium-dependent lysophosphatidylcholine transporter MFSD2A causes a non-lethal microcephaly syndrome, *Nat. Genet.* 47 (7) (2015) 814–817, <https://doi.org/10.1038/ng.3313>.
- [74] L.A.G.J.M. Vanaerts, Investigation, using rat embryo culture, of the role of methionine supply in folic acid-mediated prevention of neural tube defects, *Toxicol. Vitro* 9 (5) (1995) 677–684, [https://doi.org/10.1016/0887-2333\(95\)00070-0](https://doi.org/10.1016/0887-2333(95)00070-0).
- [75] C.N. Coelhof, N.W. Klein, Methionine and neural tube closure in cultured rat embryos: morphological and biochemical analyses, *Teratology* 42 (4) (1990) 437–451, <https://doi.org/10.1002/tera.1420420412>.
- [76] A. Hallen, et al., Mammalian forebrain ketimine reductase identified as μ -crystallin; Potential regulation by thyroid hormones, *J. Neurochem.* 118 (3) (2011) 379–387, <https://doi.org/10.1111/j.1471-4159.2011.07220.x>.
- [77] V.V. Rao, X. Pan, Y.F. Chang, Developmental changes of L-lysine-ketoglutarate reductase in rat brain and liver, *Comp. Biochem. Physiol. B* 103 (1) (1992) 221–224, [https://doi.org/10.1016/0305-0491\(92\)90435-t](https://doi.org/10.1016/0305-0491(92)90435-t).